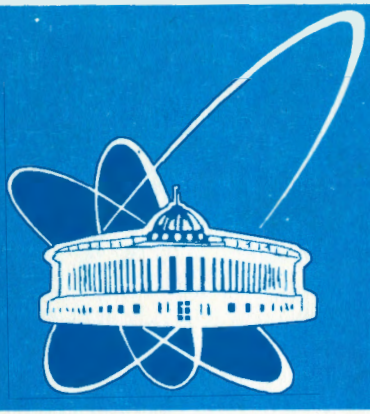

ОБЪЕДИНЕННЫЙ
ИНСТИТУТ
ЯДЕРНЫХ
ИССЛЕДОВАНИЙ

Дубна

E1-99-37

MEASUREMENT OF THE ANALYZING POWER OF THE REACTIONS $C\,(p,pp)\,X$ AND $C\,(p,pd)\,X$ AT 500 MeV

Submitted to «Nuclear Physics A»

1999

Хурэлбаатар Б. и др.
E1-99-37

Измерение анализирующей способности реакций $C\,(p,pp)\,X$ и $C\,(p,pd)\,X$ при энергии поляризованных протонов 500 МэВ

Измерены спектры совпадений и анализирующая способность $C\,(p,pp)\,X$ и $C\,(p,pd)\,X$ реакций при энергии пучка 500 МэВ. Вторичные частицы регистрировались на больших ($70°-98°$) и малых ($24{,}5°-30°$) углах. Анализирующая способность A_y в области квазиупругого pp- и pd-рассеяний качественно согласуется с соответствующей величиной для упругого рассеяния.

Работа выполнена в Лаборатории сверхвысоких энергий ОИЯИ.

Препринт Объединенного института ядерных исследований. Дубна, 1999

Khurelbaatar B. et al.
E1-99-37

Measurement of the Analyzing Power of the Reactions $C\,(p,pp)\,X$ and $C\,(p,pd)\,X$ at 500 MeV

The coincidence spectra and analyzing power in the reactions $C\,(p,pp)\,X$ and $C\,(p,pd)\,X$ were measured using a polarized beam of energy 500 MeV. Secondary particles were registered at large ($70°-98°$) and small ($24{,}5°-30°$) angles. The analyzing power in the region of quasielastic pp- and pd-scattering is in qualitative agreement with the value for elastic pp- and pd-scattering.

The investigation has been performed at the Laboratory of Particle Physics, JINR.

Preprint of the Joint Institute for Nuclear Research. Dubna, 1999

B.Khurelbaatar, V.S.Kiselev, R.Kh.Kutuev, G.Musulmanbekov, V.A.Nikitin, P.V.Nomokonov, A.V.Pavlyuk, I.A.Rufanov, R.Ya.Zulkarneev
Joint Institute for Nuclear Research, Dubna, Russia

A.D.Avezov, A.A.Gafarov, Yu.N.Koblik, V.V.Mialkovski, D.A.Mirkarimov, A.V.Morozov, V.A.Pirogov, G.A.Radyuk, B.S.Yuldashev
Institute of Nuclear Physics, Tashkent, Uzbekistan

D.Hutcheon, S.Yen
TRIUMF, Vancouver, Canada

V.Chaloupka, W.M.Dougherty, G.Liang, H.J.Lubatti, W.G.Weitkamp, T.C.Zhao
Physics Department, University of Washington, Seattle, USA

1 Introduction

The elastic and inelastic interactions of protons with nuclei have been actively investigated both experimentally and theoretically in the region of low ($T_0 < 1\ GeV$) and high energies. In particle-nucleus interactions one of the most intriguing problems is the explanation of the cross sections for production of secondary nucleons with large momentum and emission angle. They are considerably higher than expectations of models in which secondary nucleons are considered to be recoil particles produced due to rescattering of primaries or from the cascading of secondaries in a nucleus. In the region of high energies ($T_0 > 3\ GeV$) these processes are named cumulative and are interpreted in terms of quark-parton structure functions of nuclei [1, 2]. In this approach the universal function of parton distribution in nucleus is being found from experimental data.

At the energy of the present experiment, nucleons are considered as structureless particles and hadron-nucleus processes are reduced to single or multiple hadron-nucleon scattering. For example, Amado and Woloshyn [3] applied the model of single pN- scattering to the description of data [4] on production of fast protons at 180^0 in pA-interactions at primary energies 600 and 800 MeV. Their approach allowed parametrization of the high momentum part of the nucleon distribution in a nucleus. However, the investigation of two-particle spectra in the (p,2p) reaction on Li nuclei at 0.8 GeV [5] showed that this model is unsuccessful in describing angular spectra and correlations of secondary protons and there is clear indication that rescattering of struck particles by other nucleons in a nucleus has not been taken into account sufficiently.

More successful was the model of Haneishi and Fujita [6] in which it was assumed that there is a direct connection between the existence of a high momentum part of the nuclear wave function and spatially localized groups of several nucleons. This localization requires a thorough account of the interaction of nucleons in a cluster. The method of calculation was elaborated in the case of a two-nucleon cluster. However, in order to have satisfactory agreement with experimental data it was necessary to assign a model-dependent high momentum component to the Fermi motion. It was deduced from the measured nucleon distributions on the basis of a Hartree-Fock representation of nuclear wave function, but it is still unclear how many other nucleons are involved in the reaction which causes the movement of two-nucleon clusters. There are not as yet theoretical estimates of the contribution of three and more nucleon clusters in the emission of fast protons. The direct answer to these questions could be provided by an experiment where the energy and angle of several nucleons are measured in the forward hemisphere.

An additional method of investigation of the mechanism of inelastic proton-nucleus interaction is the measurement of inclusive analyzing power A_y, as was done at polarized protons energies of 500 [7] and 800 MeV [8] with the use of beryllium, carbon, nickel and tantalum targets for angles near 90^0. In the region of low energy secondary protons ($T_p < 150\ MeV$) A_y has a negative sign which may be explained

by a single pN scattering. With approach to the elastic limit for the pC reaction, A_y changes sign and reaches 0.2–0.5. Such high A_y values indicate the presence of other, less-studied coherent processes on clusters, in particular deuterons, responsible for the emission of fast particles at large angles. A correlation experiment in which the proton-proton or proton-deuteron pair is detected in coincidence could make it possible to separate this process and to study in detail its characteristics. That is the main aim of the present research.

The experimental data presented in this paper were obtained from a study of the interactions of 500 MeV polarized protons with carbon nuclei at the TRIUMF cyclotron laboratory. The correlation spectra of two particles and corresponding analyzing power of reactions $pC \to ppX$ and $pC \to pdX$ were investigated. One of the particles – a proton – was detected at angles of 70^0, 84^0 or 98^0 with an energy more than 40 MeV, and the second particle – a proton or deuteron – at angles of 24.5^0 or 30^0 on the opposite side of the beam.

One way to separate different mechanisms is to present data as the distribution of events on the plane $\{T_f, T_b\}$, where T_f, T_b are kinetic energies of the particles detected at small and large angles, respectively. For data systematization we determine the kinematical regions corresponding to single pp-interaction and to the scattering on clusters of nucleons. The cluster region (size) is determined on the basis of the energy balance. For example, if there is approximate energy balance $T_f + T_b \approx T_{beam}$ the event is considered as a single pp scattering. If $2T_f + T_b \approx T_{beam}$ scattering on a two-nucleon cluster is assumed. For each kinematic region the analyzing power

$$A_y = \frac{1}{P_{beam}} \frac{N_u - N_d}{N_u + N_d}$$

is determined. Here P_{beam} is the beam polarization normal to the scattering plane and N_u and N_d are number of events (particle pairs) detected at different P_{beam} orientations relative to the scattering plane (up and down). We follow the conventional definition of A_y: the small angle detector (detecting T_f) is located to the left of the beam.

2 Experimental set up and measuring method

The experimental set-up was a scintillation spectrometer (Fig.1) located on beamline 1B of the TRIUMF cyclotron. Its main parts, their functioning and characteristics are described below.

The target was a carbon plate 3 mm thick, turned at 45^0 to the beam axis and thus permitting detection of secondary particles emitted from the target at $\sim 90^0$. The thickness of the target was chosen according to the following requirements: the flux of particles hitting the counters from the target must be considerably bigger than that of background particles (mainly neutrons) coming from the beam dump located 5 m from the set-up, and the target must be sufficiently thin not to worsen the

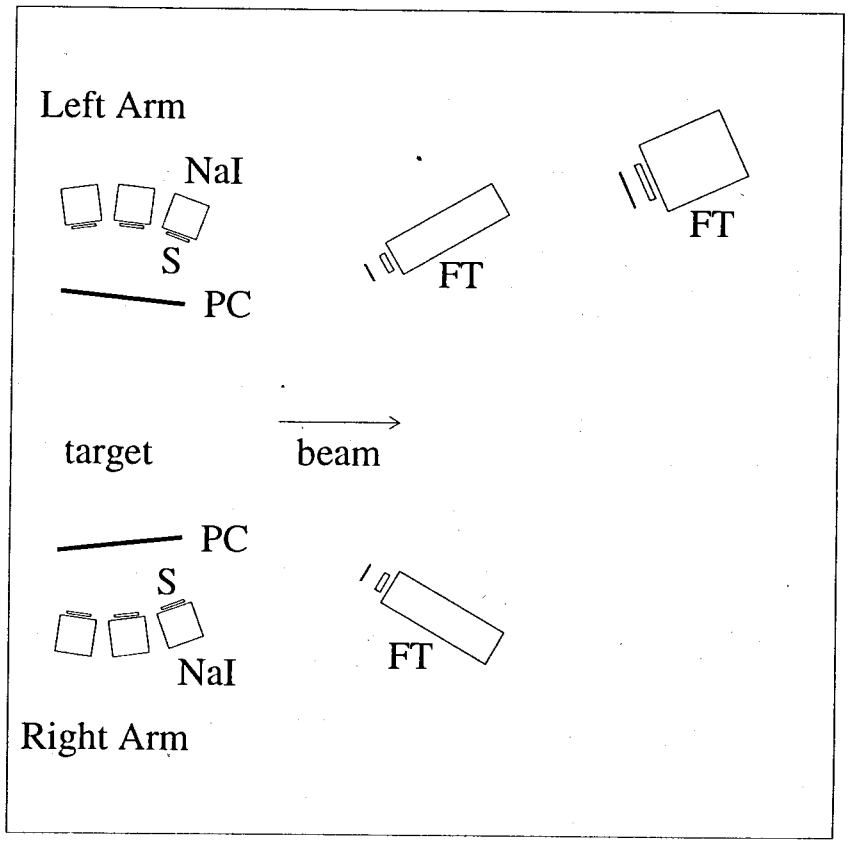

Fig. 1. Schematic view of scintillation spectrometer set-up at polarized proton beam of TRIUMF cyclotron.

PC – multiwire proportional chambers.
NaI – sodium iody scintillation counters.
S – disc scintillation counters.
FT – forward telescopes.

energy resolution of the set-up. A CH_2 target was also used for energy calibration of counters using protons from elastic pp scattering on free protons of the polyethylene.

Two mobile platforms (remotely controlled) holding the detectors were located on the left and right sides of the target. They allowed the detection of particles in the angular range $70^0 - 98^0$. On each platform two planes of multiwire proportional chambers and 8 scintillation telescopes were mounted. The telescopes were assembled into an array with the angular range $\delta\theta = \delta\phi = 14^0$, at 82 cm from the target. Each telescope consisted of a disc-shaped plastic scintillator with diameter 10 cm and thickness 1 cm and a cylindrical NaI(Tl) crystal of diameter 15 cm and thickness 15 cm. Proportional chambers with inter-wire distance 2 mm registered x, y coordinates of the particles. In the forward direction in the angular range 24.5^0 - 30^0 three telescopes were arranged. Each telescope consisted of three plastic scintillators with the thicknesses 0.5, 2.5, and 36(76) cm. They were positioned at 1.3 - 2.5 m from the target.

The event trigger was produced by coincidence of any disc scintillator and forward (2.5 cm) scintillator from opposite sides to the beam.

The electronics provided amplitude measurements of the signals from all counters and the timing of signals from plastic scintillators. (The timing of the NaI detectors was not measured.) The time resolution was 0.6 ns, after correction for its dependence on the amplitude.

The primary proton beam consisted of bunches 3 ns wide and separated from each other by 43 ns. The coincidence time of two telescopes was selected to be 70 ns. This range contained two bunches, allowing us to estimate the number of random coincidences. On average the random rate did not exceed 5% of the true coincidence rate.

The information read from the proportional chamber controller gave the width and centroid of a cluster of fired wires. The centroid of a cluster determined the x, y coordinates of the particle.

In order to control the amplification of the spectrometer electronics, light-emitting diodes (LED) were embedded in the NaI counter frames allowing the light to reach the photocathodes of photomultipliers (PM). The LEDs were equipped with stabilized pulse power supply. The control light pulses were generated at five levels in amplitude, in a wide dynamic range which spanned the range of the ADC. The pulses were generated every 5 seconds. They permitted the correction of slow and fast changes of PM amplification due to drift of beam intensity and magnetic field in the experimental hall.

The electronics (in NIM and CAMAC crates) was set up 3 - 4 m from the detectors. The read-out information was recorded event-by-event by a VAX-station connected to the detector cave through a 100 m long branch cable.

The NaI counters on their mobile platforms were calibrated with recoil protons from elastic scattering on free hydrogen in a CH_2 target. For this purpose the platforms were positioned in the range of 40^0 - 60^0. Thereafter the amplification was monitored by the LEDs. The forward thick (36 and 50 cm) counters arranged

at 24.5^0 and 30^0 were calibrated by using maximum ionization losses of protons with energies T_{max}=255 and 310 MeV, the ranges of which are equal to the respective counter thicknesses. At the same energy the amplitudes of signals in the thin (5 mm and 25 mm) counters were also determined. Later they were used for the separation of particles stopped in the thick plastic scintillator from particles which passed through it. The limited energy resolution of thin plastics made it difficult to distinguish stopped and passed protons in the T_{max}-region, and due to this low efficiency of particle identification such events were removed from further analysis.

The kinetic energy of protons stopped in a thick counter was proportional (with a small quadratic correction) to the amplitude of PM signal. For passing particles the energy was calculated by a formula deduced from the range-energy relation. The accuracy of such calculation was tested by the position of the quasi-elastic peak in two-particle spectra.

For particle identification we used the method based on the relation of ionization losses in thin and thick counters of telescope, i.e. the $(\Delta E - E)$ method. In accordance with this method signals from particles stopping in a thick counter lay along the hyperbola $\Delta E \sim m \cdot z^2/E$, where m and z are the mass and the charge of particle, respectively. The typical matrix obtained by a $S - NaI$ telescope at 70^0 is shown in Fig. 2. One may see that the protons are the main component detected. Pion and deuteron bands are also observed.

The $\{\Delta E, E\}$ matrix for the telescope at 30^0 is presented in Fig. 3. In this figure we also show the regions for stopped and passed protons, and from nuclear interactions in the plastic. The pion and deuteron lines are also indicated. To improve the quality of particle identification in forward telescopes, the time difference $t_f = \tau_f - \tau_S$ between the signals of the thick forward counter and the S counter of a $S - NaI$ telescope was used. The τ_S value was corrected for particle time of flight from target to the S - counter, taking into account the particle energy measured in the $S - NaI$ telescope. The matrix $\{t_f, E\}$ is shown in Fig.4. The marked regions correspond to those shown in Fig. 3. For further analysis we have selected only events containing protons in the S-NaI telescopes and protons or deuterons in forward telescopes. In all other coincidences much lower statistics were obtained.

The experimental data presented in this paper were obtained using an incident proton beam of average polarization 68%. The sign of polarization while data taking was reversed every several seconds, as is necessary for the measurement of the left-right asymmetry of particle emission and the calculation of the analyzing power (see Introduction). The values of $N_{u,d}$ in the formula for A_y must be normalized to equal beam intensity. For the combination of angles with $\theta_f = 30^0$ our experimental set-up is an almost symmetric polarimeter which permitted us to monitor the beam intensity at various polarizations of the beam.

The beam line has in-beam polarimeter. It provides good and continues beam polarization measurement.

The run time of data collection in this experiment was about 24 hours at a beam intensity ~0.2 nA.

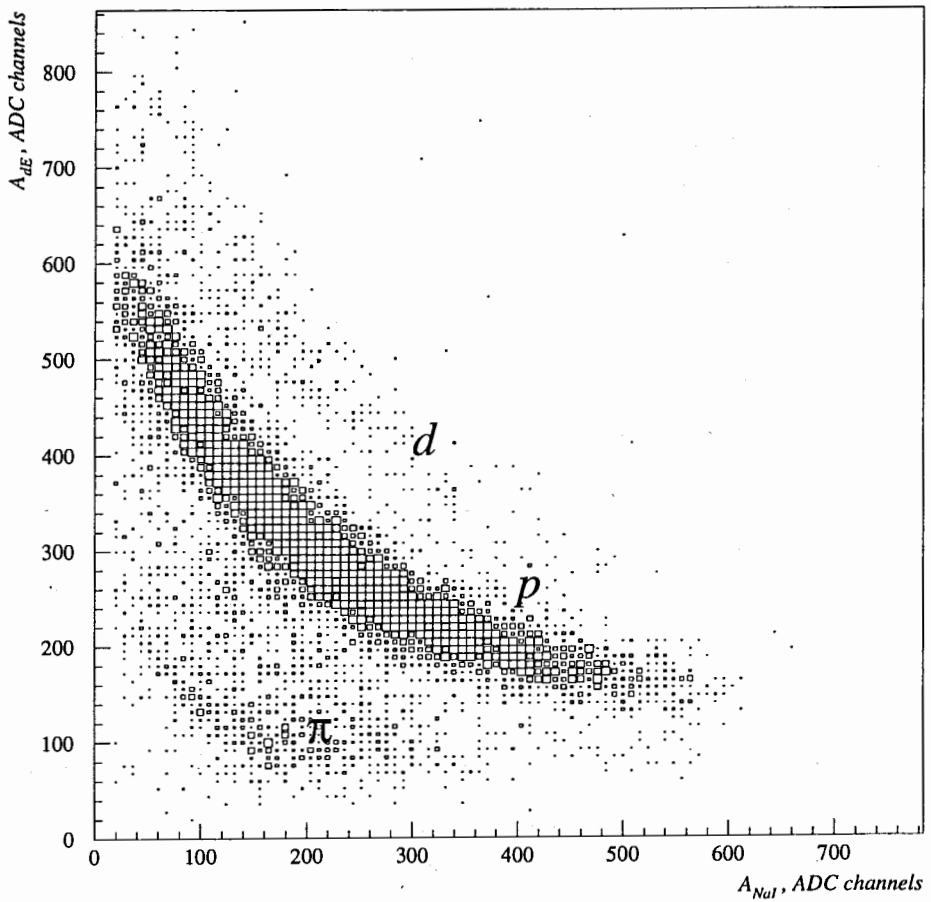

Fig. 2. $\{\Delta E, E\}$ – distribution obtained by $S - NaI$ telescope at the angle 70^0.

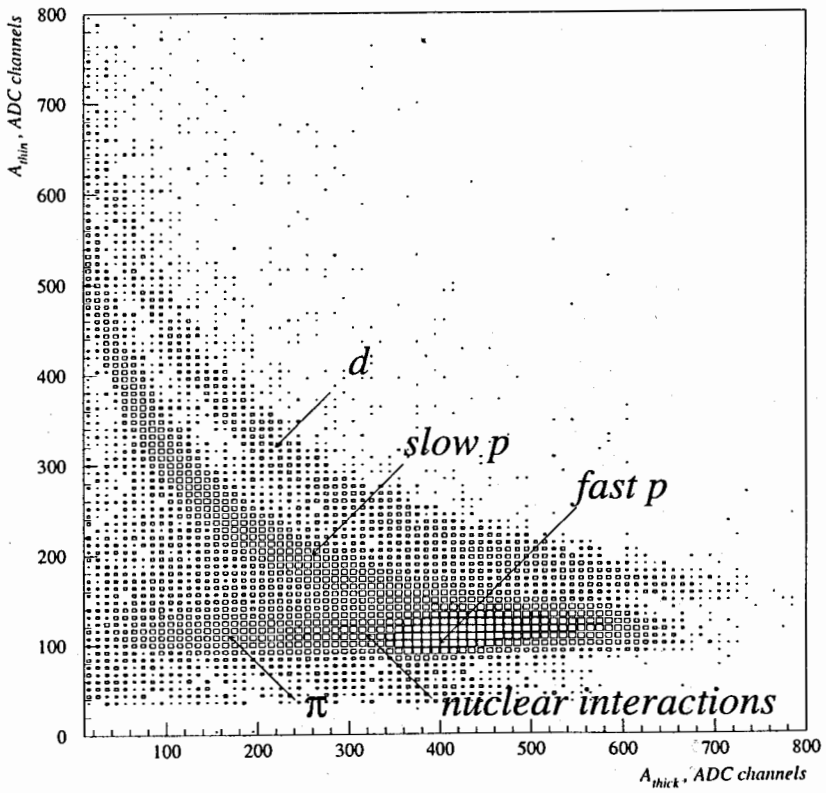

Fig. 3. $\{\Delta E, E\}$ – distribution obtained by forward telescope at 30^0.

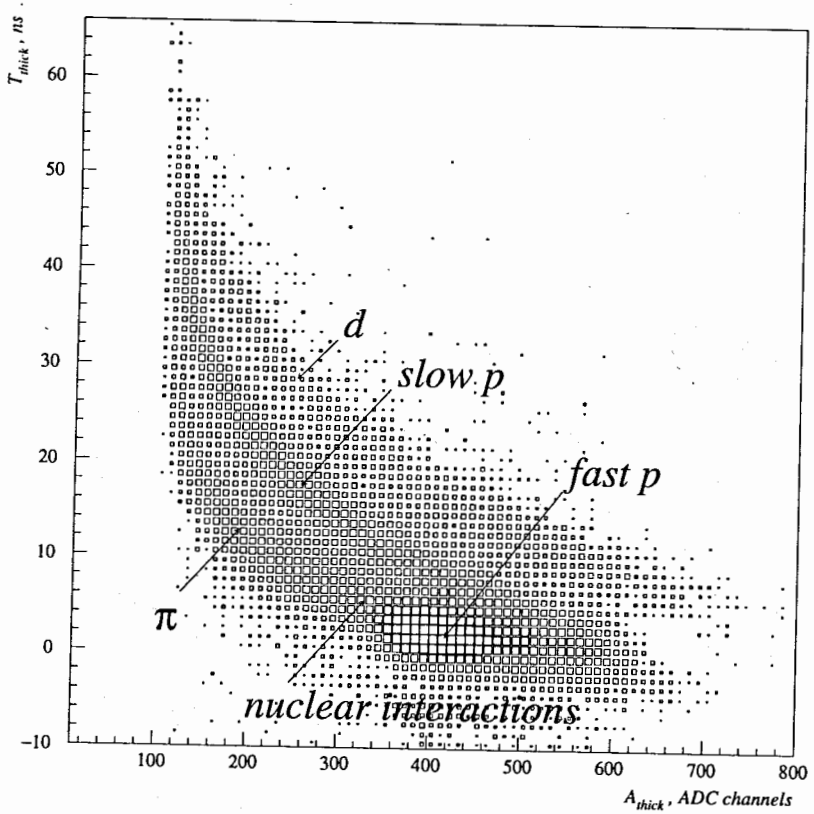

Fig. 4. $\{t_f, E\}$ – distribution obtained by forward telescope at 30^0.

3 Two-particle correlations

We measure the two-particle spectra $d^2N/dT_f dT_b$ obtained from the coincidences of particles from telescopes arranged at the angles $70, 84, 98^0$ and $24.5, 30^0$ respectively. The first group of telescopes is denoted as "b" – backward and the second group – as "f" – forward. T_b and T_f are kinetic energies of particles detected in side and forward spectrometers.

There are several types of interaction which could result in events filling the two dimensional plane $\{T_f, T_b\}$:

– Quasi-elastic pp and pd scattering in carbon. The events of this type form a well-defined group in the $T_f > 300\ MeV$ region.

– The scattering of primary protons on multi-nucleon clusters. For example, the initial proton may be scattered to an angle of 70^0 and get energy about 50 MeV, transferring to the cluster a 4-momentum squared of order $-t \approx 1(GeV/c)^2$.

– A cascade process with multiple rescattering.

It must be noted that the measured function $d^2N/dT_f dT_b$ only qualitatively corresponds to differential cross section $d^2\sigma/dT_f dT_b$ because in various regions of the $\{T_f, T_b\}$ plane the apparatus has varying detection efficiencies. This is because the particle identification in forward telescopes is done by different methods for stopping and passing particles and because of the large amount of nuclear interactions in thick counters as well.

The two-proton spectra obtained in the reaction C(p,pp)X for all combinations of measured angles are presented in Fig. 5. The dashed-dotted horizontal lines in these spectra separate the region of fast protons emitted at small angles which pass through forward counters from the region of stopped protons. For reasons mentioned above, it was impossible to identify particles and measure their energies near these lines within the band ± 35 MeV.

In each panel of Fig. 5 the yields below the dash-dotted line have been scaled up relative to those above the line, to make their features more visible; the scaling factors are given in each panel. The upper dashed lines show kinematic boundaries calculated for the quasi-elastic reaction $^{12}C(p,pp)^{11}Be$. The existence of events beyond this limit reflects the energy resolution of apparatus and the number of random coincidences.

In all spectra one may see peaks of quasi-elastic (QE) scattering, the intensity of which is sharply decreasing with the increase of angle θ_b of the large angle detector. The maxima of peaks in energy are situated noticeably lower then one would expect from kinematics. This result may serve as evidence for the production of excited ^{11}B nuclei. However, due to the systematic uncertainty in the energy calibration of forward telescopes one can not estimate the excitation energy.

One may also note some qualitative features of QE scattering. For example, at 30^0 the QE peak becomes broader with increase of θ_b. At 98^0 it has no clear lower boundary, which may be explained by rescattering of slow protons to larger angles. For events detected in coincidence with the telescope at 24.5^0, the QE peak decreases

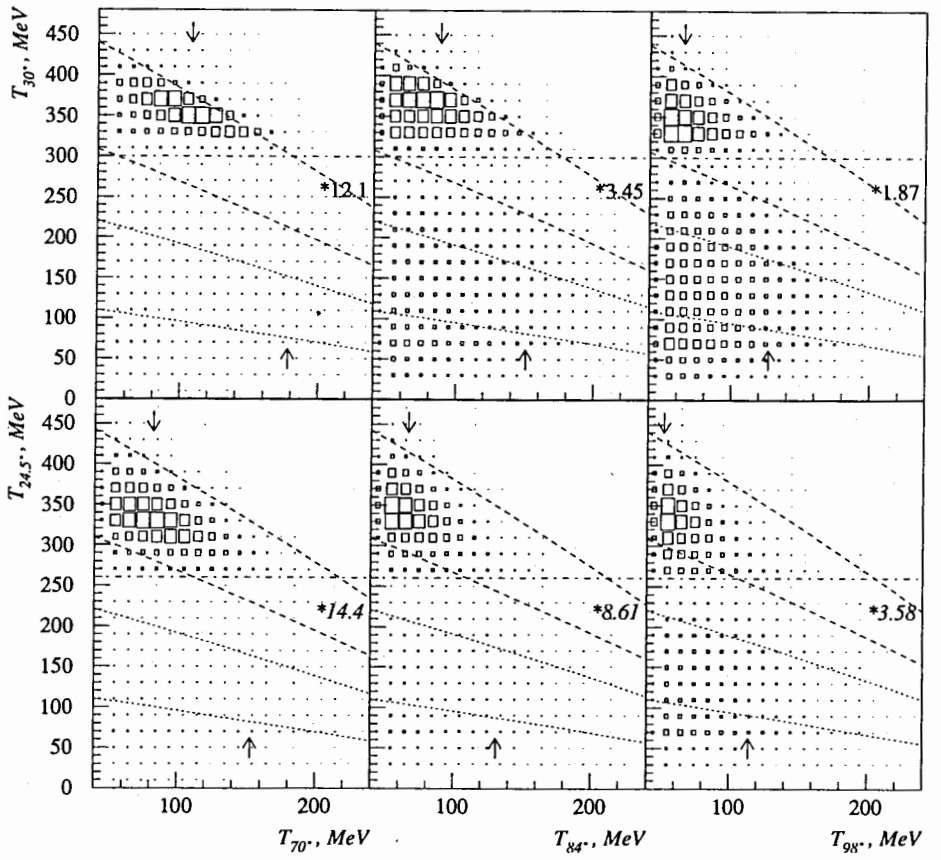

Fig. 5. Two-proton correlation spectra.
The T_θ is kinetic energy measured at angle θ.

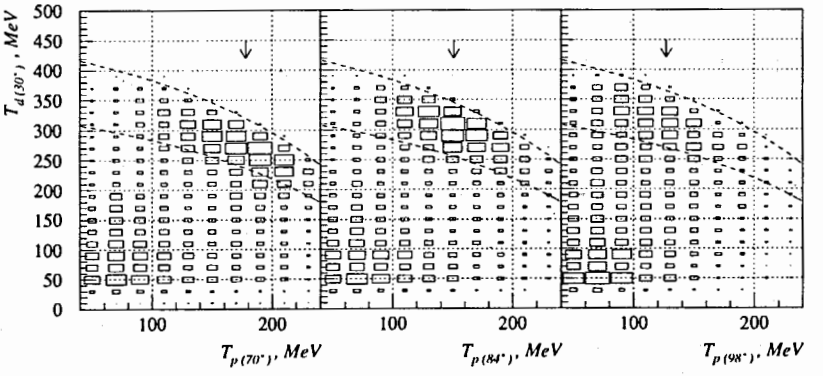

Fig. 6. Proton-deuteron correlation spectra.
The $T_{p(d),\theta}$ is kinetic energy of p or d measured at angle θ.

with θ_b more slowly than in the telescope at 30^0.

The most energetic part of the proton spectrum at large angles is accompanied by protons emitted forward and carrying a half to a third of the remaining energy, confirming the increase with angle of the contribution from scattering on two- and three-nucleon clusters in the production of fast backward protons. The arrows ↓ show position of QE peaks expected from kinematics. Pair of dashed lines indicate zone of pp-scattering. Pair of dotted lines indicate zone of p-(two-nucleon-cluster)-scattering. The arrows ↑ show expected from kinematic proton energy for proton-cluster interaction.

The two-particle pd-spectra at $\theta_f = 30^0$ for the reaction C(pd)X are presented in Fig. 6. In contrast to protons, the deuteron spectrum is confined to the region of stopping in the thick counters. As one can see from the data in Fig. 6, the QE peak as well as its energy-shift with the angle θ_b are clearly observed.

4 The kinematics of quasi-elastic reactions

Let us make a kinematic analysis of the reactions $^{12}C(p,2p)^{11}B$ and $^{12}C(p,pd)^{10}B$ for two cases shown in the diagrams in fig. 7. Here we use the following variables: $\vec{p}_0, \vec{p}_1, \vec{p}_2$ - momenta of beam and secondary particles; $\vec{p}_A$ - momentum of target nucleus; $\vec{p}_{fm}$ - the momentum of proton or deuteron on which QE scattering occurs; $\vec{p}_R$ - residual nucleus momentum. The last quantity is not measured in our experiment.

By definition $\vec{p}_R = -\vec{p}_{fm}$ in this model. The value of $\vec{p}_R$ has to be determined from momentum conservation $\vec{p}_0 = \vec{p}_1 + \vec{p}_2 + \vec{p}_R$. From the conservation of momentum and of total energy $E_0 + E_A = E_1 + E_2 + E_R$, one can obtain the relation between T_1 and T_2 (or T_f and T_b) shown in Fig. 5 by upper dotted lines. For the reaction (p,2p) the new definitions are connected with old ones as $T_1 = T_f$, $T_2 = T_b$ and for reaction (p,pd) – as $T_1 = T_b$, $T_2 = T_f$. The sum of kinetic energies $T_f + T_b$ in this case is the maximum energy which can be transferred to a pair of particles emitted at the given angles. The calculated values of Fermi momentum $p_{fm}(T_b)$ are shown in Fig.8a for (p,2p) reaction and in Fig.8b for (p,pd) reaction. The positions of minima of these functions are shown with arrows in the Figs. 5 and 6. As one can see, their values are in good agreement with the positions of QE peaks. Comparing $p_{fm}(T_b)$ for (p,2p) reaction at 70 and 98^0 one may see that the previously-noted broadening and shift of the QE band is due to the growth of p_{fm}.

The square of the energy in the center of mass and four-momentum transfer squared for QE scattering in the case of the diagram in Fig.7a are calculated by $s = (P_1 + P_2)^2$ and $t = (P_0 - P_1)^2$ where the P_i are four-momenta of the corresponding particles. The variable t is presented in Fig.9. For QE pp-scattering it depends weakly on the angle of backward particles and on energy T_2. Therefore the lines for different angles θ_2 are nearly merged. One should note that in the QE pp interaction the primary proton is scattered in a forward direction while in QE pd events the beam proton is scattered backward and that is why t strongly depends on θ_2 and T_2. The lines for different angles θ_1 24.5 and 30^0 merge with each other.

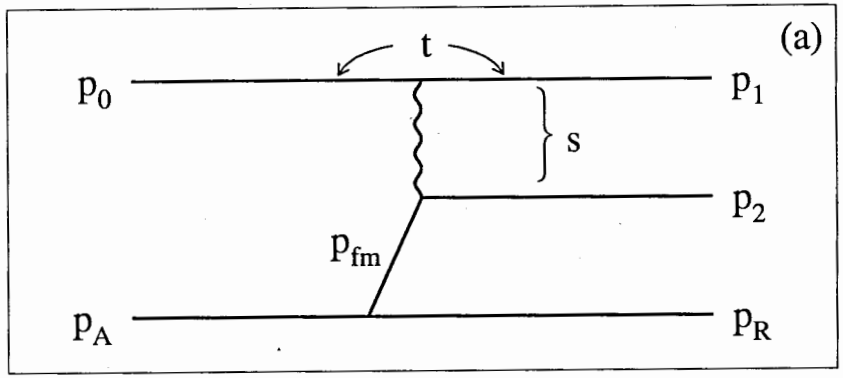

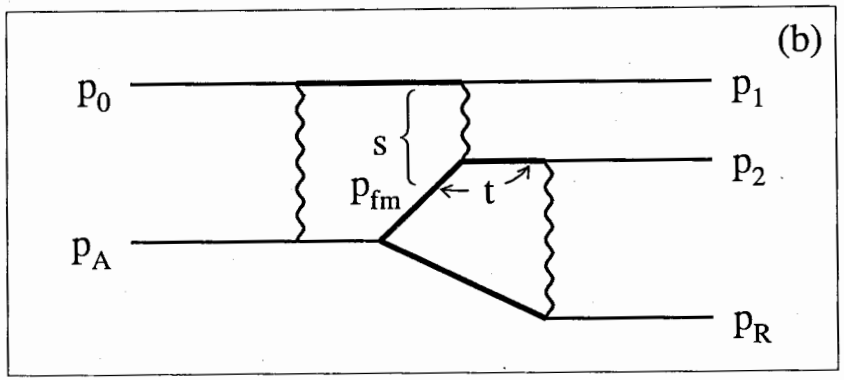

Fig. 7a. Diagram of proton-proton (deuteron) QE scattering in impuls approximation.

Fig. 7b. Diagram of proton-proton (deuteron) QE scattering with account of particle virtuality. Thick lines refer to the virtual particles (off-mass shall state).

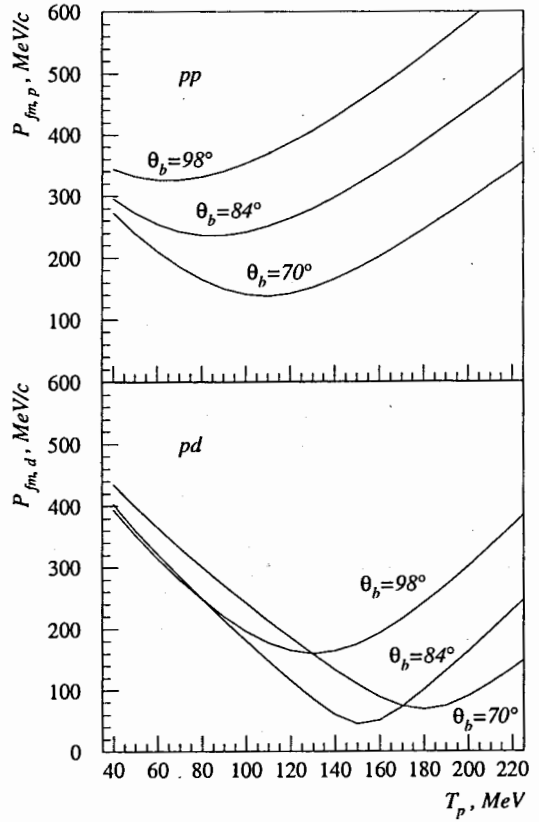

Fig. 8. Fermi momentum of internal particle for QE scattering in impuls approximation as a function of back-scattered proton kinetic energy.

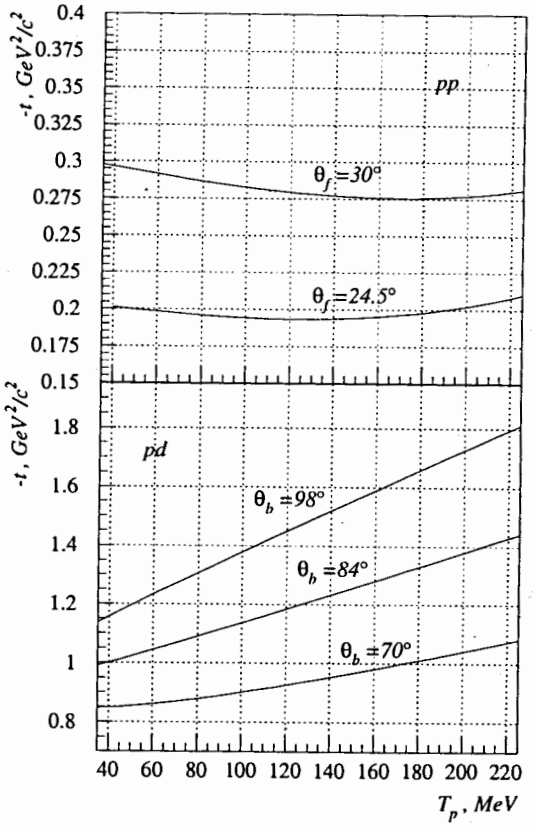

Fig. 9. Mandelshtam's t-invariant of QE scattering in impuls approximation as a function of back-scattered proton kinetic energy.

In the second case (Fig.7b) we explicitly take into account the virtuality of the particles (VP) inside a nucleus. The virtual particles are shown in Fig.7b by bold lines. The total energy of VP is equal to its total energy outside the nucleus $E_v = E$ and the mass is decreased to a bound value $m_v = m - u_0 - e_{fm}$. Here u_0 is the binding energy in the averaged field of the nucleus (for protons $u_0 = 8\ MeV$, for deuterons $u_0 = 14\ MeV$), e_{fm} is the kinetic energy of particle "2" in a nucleus before scattering – this is its Fermi motion energy $e_{fm} = \sqrt{m_{v2}^2 + p_{fm}^2} - m_{v2}$. The momentum of a VP is calculated from $p^2 = E^2 - m_v^2$. The energy of VP "2" after scattering has the value $E_{v2} = E_2 + u_0 + e_R$, where e_R is the kinetic energy of the residual nucleus. The term e_R appears because at point "A" (see Fig.7b) the VP "2" transfers to the residual nucleus the energy $e_R \approx p^2/2m_R$. The kinematic invariants are calculated as $s = (P_{v,0} + P_{v,fm})^2$, $t = (P_{v,fm} - P_{v,2})^2$. The subscript "$v$" stresses that we operate with a VP.

The analyzing power $A_{y,el}$ of elastic pp and pd scattering is calculated for the obtained values of s and t. In order to calculate $A_{y,el}$ for pp scattering we use the SAID software package of the University of Virginia [9], which calculates the value of A_y on the basis of a PWA (Partial Wave Amplitudes) approximation. For pd scattering the values of $A_{y,el}$ are determined in accordance with data from [10]. The comparison of $A_{y,el}$ with our data on A_y is shown in Figs. 10 and 12.

5 Simulation of the interactions of polarized protons with nuclei

For a better understanding of these results of the analyzing power in the reactions A(p,2p) and A(p,pd) we have developed a program for simulation of the interactions of polarized protons with nuclei. In this model the interactions of primary and secondary particles with nuclear clusters in a nucleus are taken into account. In the framework of our model the hadron-nucleus interaction is considered as a sequence of elastic and inelastic nucleon-nucleon collisions, i.e. as a basic idea we choose the intranuclear cascade approach [11]. The target nucleus is considered as a Fermi gas of nucleons confined in a certain volume with a diffuse boundary. It is assumed that the nucleons are in a potential well $V(r) = u_0 + p_{fm}^2/2m$, where m - mass of free nucleon, u_0 – averaged binding energy in nucleus, p_{fm} – Fermi momentum of nucleon in a nucleus. The influence of the nuclear potential on the particle entering the nucleus appears as an instantaneous increase in its kinetic energy by the value of V(r). The kinetic energy of relative motion of colliding particles is calculated taking into account the Fermi motion of intranuclear nucleons. The probability of any two-particle collision is determined by the cross section of the nucleon-nucleon or pion-nucleon interaction and by the number of nucleons which are confined within a cylinder with a radius $r_{int} = r_0 + \lambda$, where $r_0 = 1.3\ fm$ and λ is the wavelength of the tracked particle. The cylinder axis is directed along the vector of particle velocity and the probability of being scattered by the k-th nucleon is determined

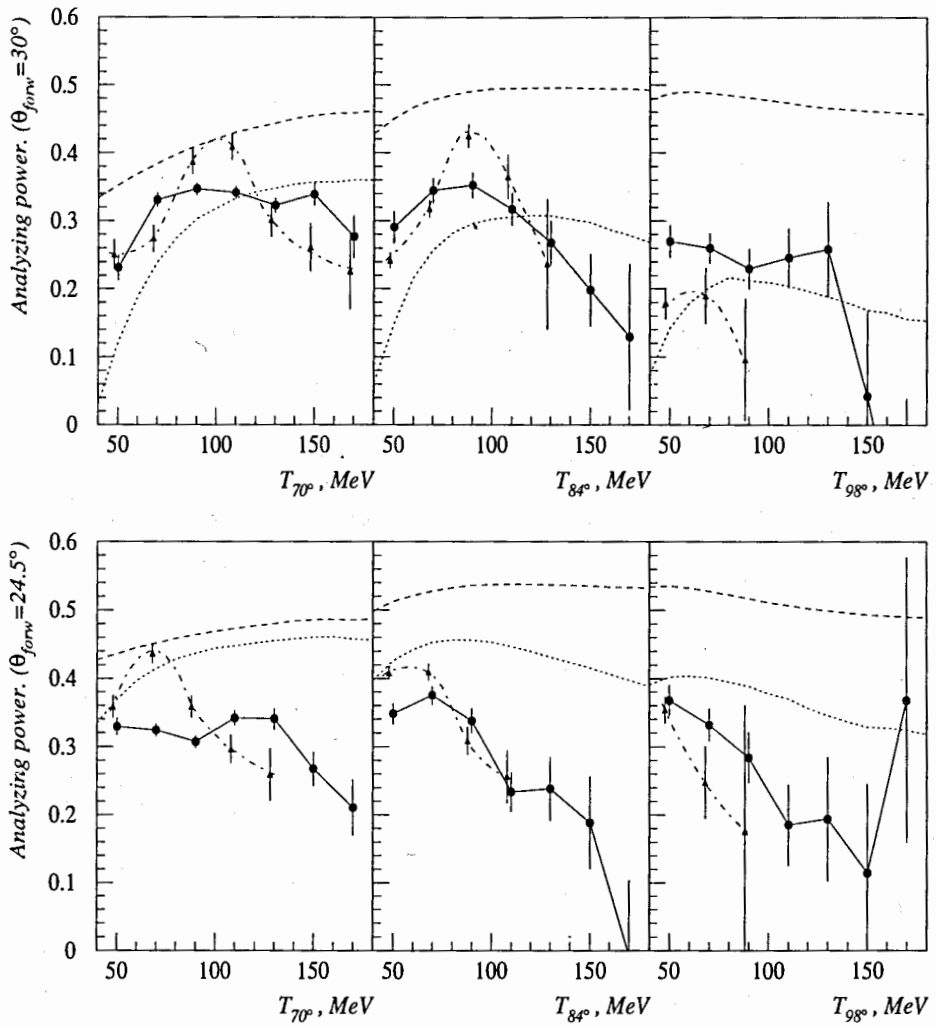

Fig. 10. Analysing power vs proton energy for QE pp scattering.

- • – Data of this experiment.
- - - - – Calculation in impuls approximation.
- ..... – Model of single scattering on virtual proton.
- ▲ – Cascade model with clusters.

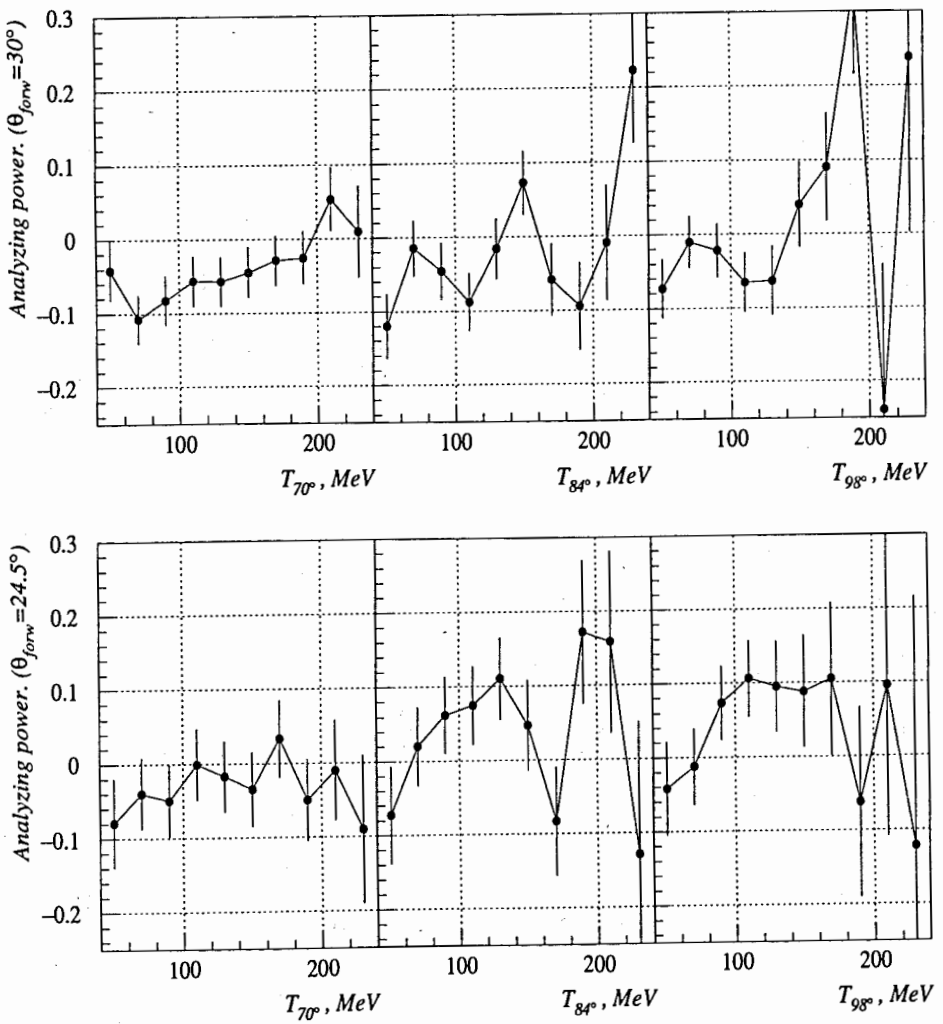

Fig. 11. Analysing power vs proton energy for pp coincidences with $k = 2$.

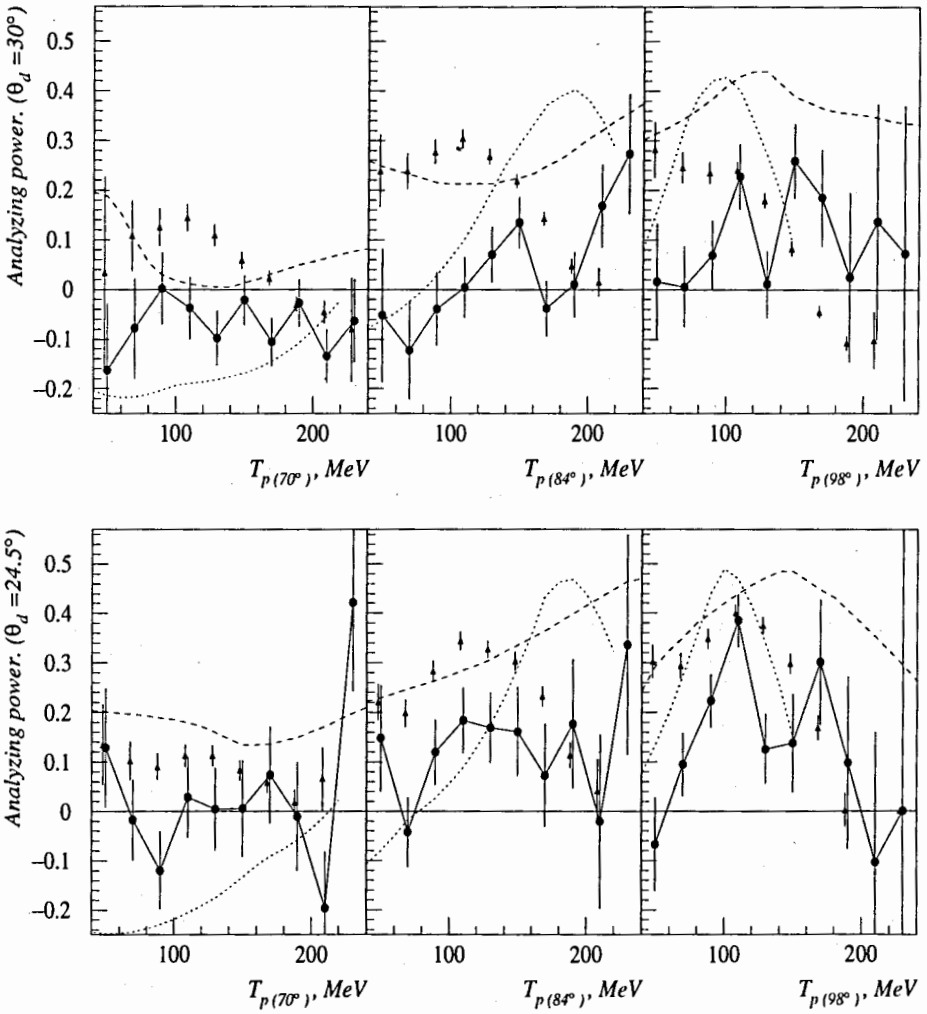

Fig. 12. Analysing power vs proton energy for QE pd scattering.

- • – Data of this experiment.
- - - - – Calculation in impulse approximation.
- ..... – Model of single scattering on virtual proton.
- ▲ – Cascade model with clusters.

by a binomial distribution $w_k = \prod_{i=1}^{k}(1-q_i)q_k$, where the partial probability q_i (i=1,2...) is expressed through the interaction cross section on i-th nucleon σ_i: $q_i = \sigma_i/\pi(r_0+\lambda)^2$. The coordinates of nucleons are generated in accordance with a standard distribution of nuclear density: $\rho(r) = \rho_0 \exp(-r^2/R_0^2)$, $R_0 = r_0 A^{1/3}$ for $A < 10$ and $\rho(r) = \rho_0/(1+\exp((r-a)/b))$ for $A > 10$. Here the radius of half density is a = 1.07A fm and the diffuseness parameter of the boundary is b = 0.545 fm. The pointlike nucleons in the nucleus are subject to a "nuclear core" condition: $d \geq 2r_{cor}$, where d is the relative distance between nucleons, and $r_{cor} = 0.4\ fm$ – the minimum possible distance between the nucleons. For the momentum distribution of nucleons the assumption of a Fermi gas with zero temperature and isotropy in space $w(p)dp \sim pdp$, $0 < p < p_{max}(r)$ is made. The maximum momentum is expressed through the nuclear density $p_{max}(r) = (3\pi^2)^{1/3} h \rho^{1/3}(r)$.

For two-particle collisions in a nuclear cascade all kinematic characteristics are calculated. The Pauli principle is checked, i.e. the final nucleon momentum in a given collision must be more than p_{max}. The particles inside the nucleus are tracked down to a minimum kinetic energy $T_{min} = V(r) + T_{cut}$. It is assumed that a particle with less energy is absorbed by the nucleus but one having higher energy continues to participate in the cascade or escapes the nucleus. $T_{cut} = V_c(r)$ for pions and $T_{cut} = V_c(r) + u_0$ for nucleons, where $V_c(r)$ is the Coulomb energy of the particle at the outer boundary of nucleus.

When simulating proton-nucleus interactions it was assumed that clusters consisting of two and three nucleons are formed in the nucleus with a certain probability [12]. When simulating the reaction A(p,2p) we assume these clusters fragment into their constituents after the first interaction. In the reaction A(p,pd) the cluster (deuteron) escapes the nucleus without decay.

To describe scattering of polarized protons on a nucleus, the analyzing powers $A_{pp}(\theta, T)$ and $A_{pd}(\theta, T)$ pp and pd interaction are introduced in the simulation program. Their values are taken from experimental data obtained for pp and pd scattering [10, 13, 14, 15]. The differential cross-section of QE scattering on an intra-nuclear nucleon is determined by the formula:

$$d\sigma(\theta,\phi,T)/(d\omega dT) = d\sigma(\theta,T)/(d\omega dT) \cdot (1 + A(\theta,T)(\vec{P}_{beam} \cdot \vec{n})),$$

where $\vec{n}$ – vector normal to the reaction plane, $\vec{P}_{beam}$ is the polarization of the primary particle.

6 The analyzing power measurement

The experimental two-particle spectra are divided to kinematic zones corresponding to clusters of size k on which the interactions take place. (k is the number of nucleons in the cluster.) The value of k is determined as a ratio of maximum possible energy to the energy which is taken away by the proton scattered at a small angle: $k = (T_{beam} - T_b - k \cdot u_0 - T_{rec} - E_{exit})/T_f$, where u_0 is the nucleon binding energy in a

nucleus, T_{rec} – kinetic energy of recoil nucleus, E_{exit} – excitation energy of residual nucleus. The zones corresponding to the scattering on quasi-free protons (k=1) and on two-nucleon clusters (k=2) are shown by dashed and dotted lines respectively in Fig. 5. The band width on T_f is taken equal to ± 15% of T_f. For the events in these zones the analyzing power is presented in Fig. 10 for k=1 and in Fig. 11 for k=2. It should be noted that the sign of A_y for the case k=1 is determined by the forward-scattered proton in a QE reaction description. Assuming that for $k > 2$ the primary proton scatters backward, the sign of A_y is determined by the proton scattered at the larger angle. Accordingly, in Fig 12 where the analyzing power of QE pd scattering is presented, the value of A_y is determined by the more backward-scattered proton. The corresponding kinematic region is shown by a dashed line in Fig. 6.

In all presented data only statistical errors are shown. The systematic error may come from poor energy resolution of forward telescope. In the energy interval $180 \geq E \geq 300\ MeV$ slow (stopped in thick counter) and fast (punch through) particles may be mixed up due to poor energy resolution of the ΔE-counter and nuclear interactions in E-counter. The evaluation of systematic error is done by means of GEANT - simulation particles detection in forward telescopes. It is shown that contamination of slow particles by fast one is less then 6 %. Assuming left-right symmetry of the fast particles emission we conclude that A_y may by systematically decreased on 0.06.

7 Discussion of results

At primary energy about 500 MeV, where the excitation of quark degrees of freedom is not noticeable, the proton-nucleus interactions can be described in terms of the nucleon wave function of a nucleus. The investigation of the emission of fast protons at large angles gives the possibility of obtaining information about the high momentum components of nucleons and their correlated states. The kinematic region chosen in our experiment allows both phenomena to be studied if their cross sections are comparable.

The direct evidence for the existence of high momentum nucleon components in a nucleus comes from the presence of QE peaks in two-proton spectra. In our experiment this reaction channel is traced for an intra-nuclear nucleon momentum from 100 to 300 MeV/c. The nature of these deep off-mass-shell states is not well studied or understood. Can they be explained by the common nuclear potential or is it necessary to account for collective states of several nucleons?

We interpret the analyzing power data using the three models: the impulse approximation (diagram in Fig. 7a), a single scattering taking into account the particles' virtuality (diagram in Fig. 7b) and a cascade model, which accounts for the particles' virtuality and rescattering. The impulse approximation results deviate from the experimental data by 0.20 to 0.40. The virtuality account reduces the disagreement to 0.20. The cascade model gives the best description of the data. It is in qualitative agreement with experimental data for $A_y(pp)$, as shown in Fig. 10.

In the previous study [16] the quantity A_y has been measured in inclusive reaction C(p,p) at beam energy 280 MeV and 420 MeV. It was found that $A_{y,inclus} \approx 0.1 - 0.15$ and it is noticeably less then corresponding value for elastic scattering $A_{y,el} \approx 0.25 - 0.35$. This reduction of $A_{y,inclus}$ is, perhaps, due to contamination of QE peak by cascade particles and due to averaging of $A_{y,inclus}$ over wide interval of s and t.

The knocking out of deuterium may be of more interest for investigation of collective states of nucleons in nucleus. The scattering on correlated pairs of nucleons can imitate the scattering on deuterium in a nucleus. And the difference of $A_y(pd)$ from the analyzing power for the free pd interaction may give information about pair states of nucleons in nuclei. The simplest interpretation this reaction is QE scattering. Its analogue is pd backward scattering, for which many $A_{y,el}(pd)$ measurements have been done.

In the two-particle spectra shown in Fig.6, one can observe the events corresponding to the QE knock-out of deuterons at Fermi momenta of deuteron-like states in nucleus from 50 to 300 MeV/c and 4-momentum-transfer squared of $0.9-1.7\ (GeV/c)^2$. The peak has an almost symmetrical form, thus attesting to the small influence of rescattering. The low background under the peak indicates also that scattering on a cluster consisting of three or more nucleons, the fragment of which might be the deuteron, is of rather low probability. The value of A_y for the QE reaction is shown in Fig. 12. Again the cascade model gives the best description of the data, although there are deviations of about 0.2. This may be evidence for a difference between the two-nucleon cluster wave function in a nucleus and that of the free deuteron. Unfortunately, due to the relatively large statistical errors it is difficult to make quantitative conclusions on the basis of the observed behavior of A_y as a function of T_b. However the data may be useful for comparison with predictions of different models. Among them one can mention a number of versions of distorted-plane wave impulse approximation – DWIA (see, for instance [17]) and its relativistic version [18]. In these approaches the waves corresponding to ingoing and outgoing particles are considered as distorted-plane waves. The distortion is obtained by taking them as solution of Schredinger or Dirac equation, with complex optical potential. This is effective accounting for the large number of degrees of freedom of the target nucleus. The polarization P in QE reaction $^{40}Ca(p,2p)$ at T_{beam}=500 MeV and $\theta_f = 15.5^o$ is calculated in [18]. It is P=0.35 – 0.45 and weekly depends on QE peak position. This value qualitatively agrees with our result. For exact comparison one needs to perform calculation for concrete kinematics of the experiment.

It is well known that nuclear structure effects influence the (p,2p) polarization (and so analyzing power) [20]. For example, the protons struck from the shells $P_{3/2}$ and $P_{1/2}$ have the opposite sign of polarization. Our value of A_y is averaged over all nuclear shell states due to lack of the apparatus energy resolution. Cascade model which we use operates with Fermi-gas and neglect nuclear structure effects. It is surprise why crude model so successful in data description.

The region k=2 for pp spectra is also relevant for investigation of correlated states. In the case of decay of a two-nucleon cluster knocked forward, we detect a

proton with half the total cluster kinetic energy on average. In Fig. 5 the energy of a proton corresponding to minimum Fermi momentum of a nucleon pair $T_{2,min}$ is shown by an upward-pointing arrow. At $T > T_{2,min}$ the slump of pp spectrum in the k=2 zone is exactly of the same type as for the QE pd distribution as function of T_b. This similarity is an indirect prove that primary proton strikes two-nucleon cluster. The filling of the spectrum at lower T_b values is due to background from rescattering and fragmentation of the nucleus.

The contribution of rescattering to pp correlation spectra was also studied by Miaki et al. [19]. For this purpose in addition to a pair of counters placed in one plane, another detector pair at azimuthal angle $\phi = 90^0$ was used. After subtraction of this spectrum from the coplanar one, the peak were observed with decreased background.

Our data also show that the analyzing power measured in the k=2 zone of the pp spectrum does not exceed 0.10 – Fig. 11. There is an increase of A_y with increase of θ_b. This kinematic region may be populated by events from a superposition of cluster decay and pN-interaction with further rescattering.

8 Conclusion

In this paper we have presented the first results of the measurements of the analyzing power in reactions with QE knocking out of deuterons in proton-nucleus interactions. Also we have measured the analyzing power of proton emission at large angles, which corresponds to proton Fermi momentum in the nucleus in the range of 100–300 MeV/c. Similar result has been obtained in [20] for the reaction $^{16}O(p,2p)$ at energy 200 MeV.

The experimental two-particle spectra allow determination of a kinematic boundary between two mechanisms of proton emission at large angles: single pN interaction and scattering on two-nucleon clusters. The first mechanism prevails for nucleon Fermi momentum $p_{fm} < 200\ MeV/c$. In the region $p_{fm} > 200\ MeV/c$ the events corresponding to rescattering and scattering on two-nucleon clusters are dominating. The observed pd correlation spectra indicate that the incident proton in most cases is scattered on two-nucleon clusters but not on one of three or more nucleons. We observed peaks of QE pd scattering which were well distinguished from background and non-distorted (symmetrical) up to 350 MeV/c Fermi momentum of two-nucleon clusters and this result can serve as direct evidence for the presence of high-momentum components in Fermi motion. The alternative explanation of nuclear hardness in terms of spatially localized multi-nucleon clusters with normal Fermi distribution seems to us less justified in view of our data. We believe that the results will be useful in investigation of nuclear wave functions.

We would like to thank Professors J-M.Poutissou, E.Vogt and I.A.Savin for support in performing this experiment. We also extend our thanks to L.Barabash, V.Budilov and A.Laricheva for assistance in equipment preparation. Our special acknowledgments are addressed to the staff of TRIUMF laboratory for their com-

prehensive help during the runs of this experiment; in particular, we thank Grant Sheffer for his help in assembling electronics.

References

[1] A.M.Baldin. Elementary Part. and Atomic Nucl., v. 8, num. 3, p. 429, (1977).

[2] A.V.Efremov. Elementary Part. and Atomic Nucl., v. 13, num. 3, p. 613, (1982).

[3] R.D.Amado and R.M.Woloshyn. Phys. Rev. Lett., 36, 1435 (1976).

[4] S.Frankel et. al. Phys. Rev. Lett. 36, 642 (1976).

[5] H. Brody et.al. Phys. Rev. C 24, 2157 (1981).

[6] Y.Haneishi and T.Fujita. Phys. Rev. C 33, 260 (1986).

[7] G.Roy et.al. Phys. Rev. C 23, 1671 (1981).

[8] S.Frankel et.al. Phys. Rev. Let. 41, 148, (1978).

[9] http://clsaid.phys.vt.edu/ CAPS/

[10] A.N.Anderson. Phys. Rev. Let. 40, 1553, (1978).

[11] V.S.Barashenkov et. al. Uspekhi Fiz. Nauk. v. 109, 91, (1973).

[12] T.Fujita Phys. Rev. Lett. 39, 174 (1977).

[13] O.Chamberlain Phys. Rev. 105, 288 (1957).

[14] M.L.Barlett et. al. Phys. Rev. C 27, 682 (1983).

[15] J.A.Marshall et. al. Phys. Rev. C 34, 1433 (1986).

[16] C.Chen et. al. Nucl. Phys., A510, 713, (1990).

[17] E.Rost et.al. Phys. Rev. C35, 687, (1987).

[18] C.J.Horowitz et. al. Phys. Rev. C37, 2032, (1988).

[19] Y.Miaki et.al. Phys. Rev. C 31, 2168 (1985).

[20] P.Kitching et. al. Nucl. Phys., A340, 423, (1985).

Received by Publishing Department
on February 15, 1999.